A Study on Image Change Detection Methods for Multiple Images of the Same Scene Acquired by a Mobile Camera

Guntur Tanjung

School of Mechanical Engineering

The University of Adelaide

South Australia 5005

Australia

A thesis submitted in fulfilment of the requirements

for the degree of Doctor of Philosophy in

Mechanical Engineering

on the 12th October 2009

CHAPTER 5

AUTOMATIC IMAGE REGISTRATION AND REGIONS OF INTEREST EXTRACTION

Chapter 5 describes an algorithm utilized to register input images into the same coordinate system with the reference image. CPs extracted from the reference image and each input image, as mention in Chapter 4, are used as correspondence points in this image registration. Outputs of image registration are registered input images. This chapter also explains how to extract automatically regions of interest from the reference image and registered input images using information of registered input images.

5.1 Background

Two images of the same scene captured by a camera from slightly different positions, angles and at slightly different times will produce displacements of same objects (parallax) in the two images (Russ, 2002). The first and second images are referred as the reference image and input image. This parallax problem can be solved by adjusting geometric of the two images (Goshtasby, 2005; Radke *et al.*, 2005). The geometric adjustment of two images of the same scene works properly when the two images are flat plane images such as satellite images used in the remote sensing community, and magnetic resonance (MR) and positron emission tomography (PET) images utilized in the medical community Goshtasby, 2005).

When two images of the same scene are depth plane images, like surveillance images captured by a mobile camera in which position of the camera is perpendicular towards the scene, no matter how image registration is undertaken, the displacement of the same points in the reference image and the registered input image presents the disparity / range (Russ, 2002). Depth plane images are used in this research. The purpose of image registration in this research is to reduce displacements of same

objects in the reference image and input images especially left and right posts of the wire fence.

5.2 Algorithm Overview

The following steps are established in order to register the AOI1_RI and every AOI1_II discussed in Chapter 4 and to extract new regions of interest from the AOI1_RI and registered AOI1_IIs based on information of registered AOI1_IIs.

1. Read CPs extracted from the AOI1_RI,
2. For every AOI1_II
   2.1 Read CPs extracted from the AOI1_II,
   2.2 Estimate parameters of the linear conformal (similarity) transformation such as scaling, rotational, and translational differences between the AOI1_RI and AOI1_II respectively, based on information of two pairs of the correspondence points. The similarity transformation is based on the equations below.

$$X = s\,x\cos(\theta) - s\,y\sin(\theta) + h \tag{5.1}$$

$$Y = s\,x\sin(\theta) + s\,y\cos(\theta) + k \tag{5.2}$$

   where s, θ, and (h, k) are the scaling, rotational, and translational differences between the AOI1_RI and AOI1_II.
   2.3 Transform and re-sample the AOI1_II based on the estimated linear conformal transformation in order to generate the registered AOI1_II (RAOI1_II).
   2.4 Extract a region of interest (ROI) of the AOI1_RI (ROI2_RI) and a ROI of the RAIO1_II (ROI2_II) based on information of the RAOI1_II.

5.3 Experimental Results and Discussion

To decrease computational time of registering the AOI1_RI and AOI1_IIs, CPs extracted from the AOI1_RI can be processed once in advance and they can be saved in a text file (*.txt). Thus, reading CPs extracted from the AOI1_RI can be performed continuously into the text file.

Figs. 5.1 (a), 5.1 (b) and 5.1 (c), below, depict the registered AOI1_II-1 (RAOI1_II-1), registered AOI1_II-5 (RAOI1_II-5), and registered AOI1_II-9 (RAOI1_II-9).

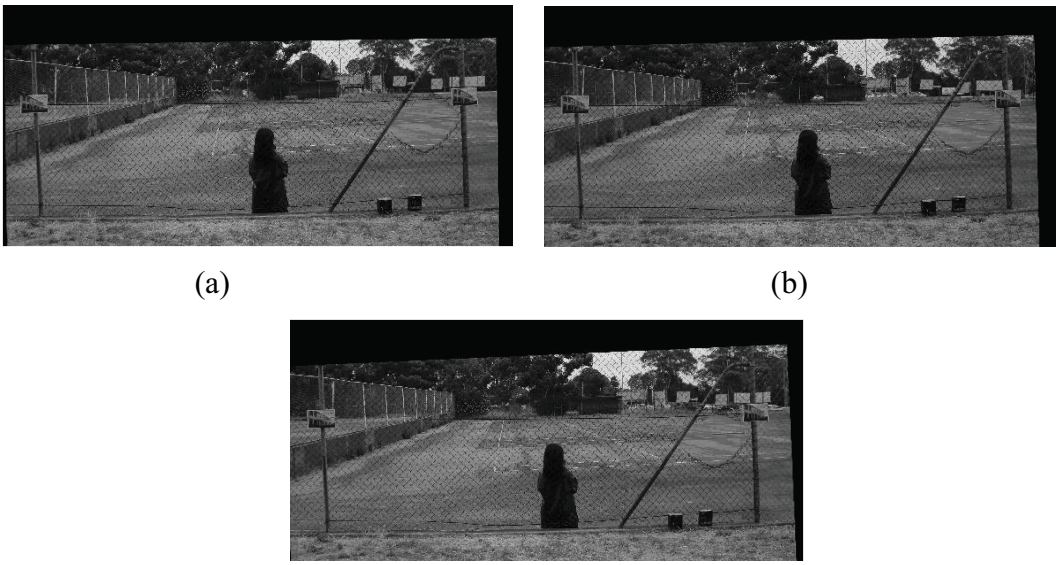

(a) (b)

(c)

Fig. 5.1 The RAOI1_II-1 (a), RAOI1_II-5 (b) and RAOI1_II-9 (c)

As seen in Figs. 5.1 (a), 5.1 (b) and 5.1 (c), there are two different regions: a region with information (objects) on it and a region without information (the black region) on it- in every image. For further process, the information region must be separated from the black region.

The followings explain how to separate the information and black regions from each RAOI1_II, for example the RAOI1_II-1 in Fig. 5.1 (a). Firstly, the RAOI1_II-1 is converted into a binary image by using the following rule:

$$B(x,y)=\begin{cases}1 & if\ \text{RAOI1\_II-1}\ (x,y) > 0\\ 0 & if\ \text{RAOI1\_II-1}\ (x,y) = 0\end{cases} \tag{5.3}$$

where B(x, y) is a binary image of the RAOI1_II-1 and RAOI1_II-1 (x, y) represents a pixel value for coordinates (x, y). As a result of the image thresholding, the binary image contains white and black areas. The white area was referred to as the bounding box. Secondly, the bounding box parameters such as the coordinate of the upper left corner, width and height are extracted from the B(x, y). Based on these bounding box parameters, the region of interest is finally cropped from the RAOI1_II-1 (i.e.,

ROI2_II-1). Moreover, the region of interest of the AOI1_RI is also cropped automatically based on information of the bounding box parameters (i.e., ROI2_RI-1). The reason of cropping the RAOI1_II-1 and AOI1_RI by using the same bounding box parameters is to ensure that the ROI2_II-1 and ROI2_RI-1 are in the same size in pixels. Figs. 5.2 (a) and 5.2 (b) depict the ROI2_II-1 and ROI2_RI-1 respectively.

(a) (b)

Fig. 5.2 The ROI2_II-1 (a) and ROI2_RI-1 (b). Both images are cropped automatically based on the same bounding box parameters extracted from the RAOI1_II-1

The same regions of interest extracting steps as explained above are established to all RAOI1_IIs. Figs. 5.3 (a) and 5.3 (b), below, depict the ROI2_II-5 and ROI2_II-9 extracted from the RAOI1_II-5 and RAOI1_II-9 based on information of their own bounding box parameters.

(a) (b)

Fig. 5.3 The ROI2_II-5 (a) and ROI2_II-9 (b) extracted from the RAOI1_II-5 and RAOI1_II-9 by using information of their own bounding box parameters

Figs. 5.4 (a), 5.4 (b) and 5.4 (c), below, depict the RAOI1_II-2, RAOI1_II-6 and RAOI1_II-10.

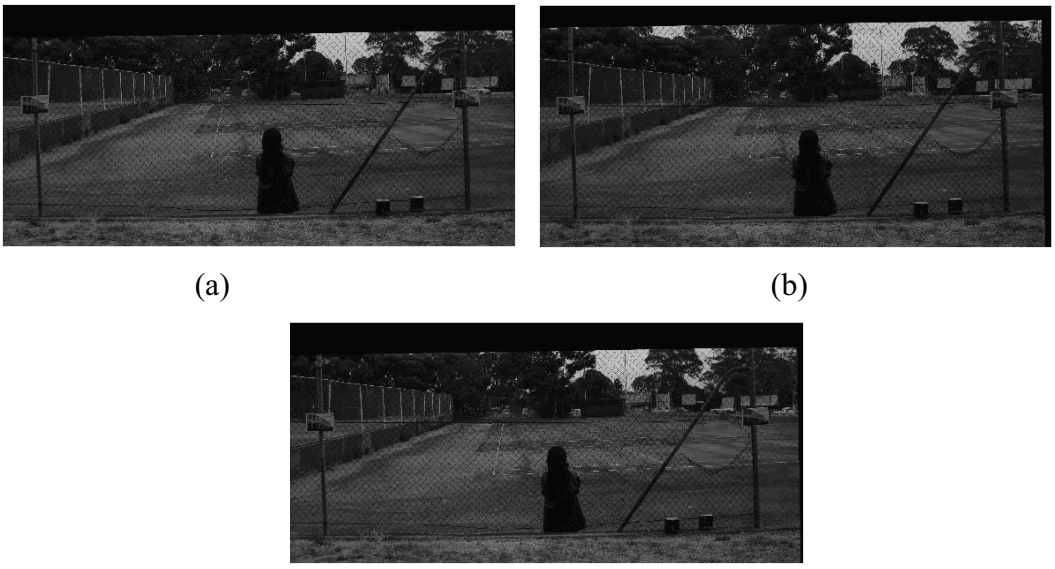

(a) (b)

(c)

Fig. 5.4 The ROI1_II-2 (a), ROI1_II-6 (b) and RAOI1_II-10 (c) produced after performing image registration by using their CPs

Information and black regions in images in Figs. 5.4 (a), 5.4 (b) and 5.4 (c) are then separated based on information of their bounding box parameters extracted from their images. Figs. 5.5 (a), 5.5 (b) and 5.6 (c), below, depict the ROI2_II-2, ROI2_II-6 and ROI2_II-10 respectively.

(a) (b)

(c)

Fig. 5.5 The ROI2_II-2 (a), ROI2_II-6 (b) and ROI2_II-10 (c) extracted from the RAOI1_II-2, RAOI1_II-6 and RAOI1_II-10 by using their bounding box parameters

Figs. 5.6 (a), 5.6 (b) and 5.6 (c), below, depict the RAOI1_II-3, RAOI1_II-7 and RAOI1_II-11. Information regions of images in Figs. 5.6 (a), 5.6 (b) and 5.6 (c) are then separated from black regions in creating the ROI2_II-3, ROI2_II-7 and ROI2_II-11 (see Figs. 5.7 (a), 5.7 (b) and 5.7 (c), below).

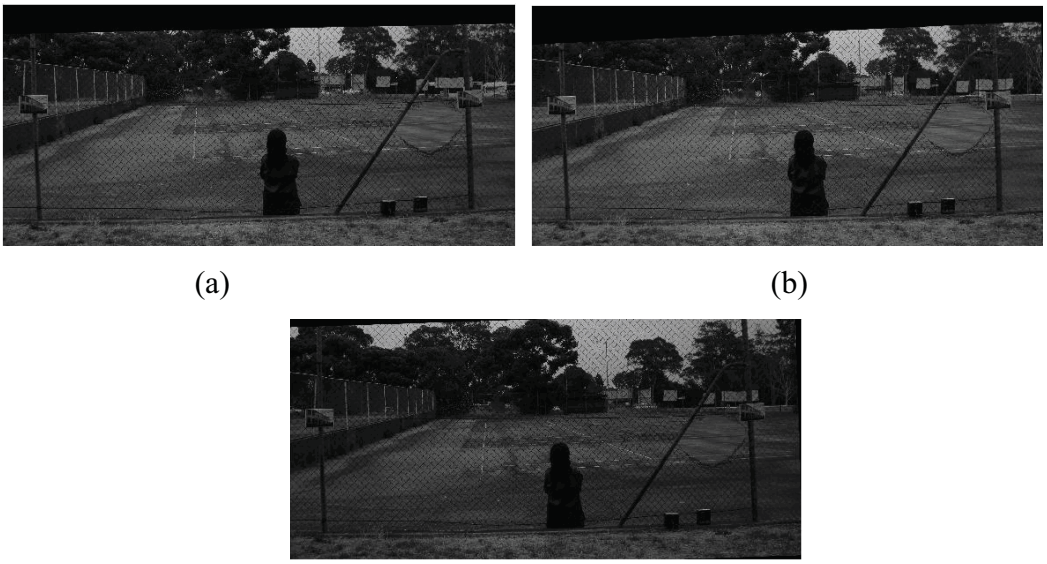

(a) (b)

(c)

Fig. 5.6 The registered AOI1_II-3 (a), registered AOI1_II-7 (b) and registered AOI1_II-11 (c) after performing image registration by using their CPs

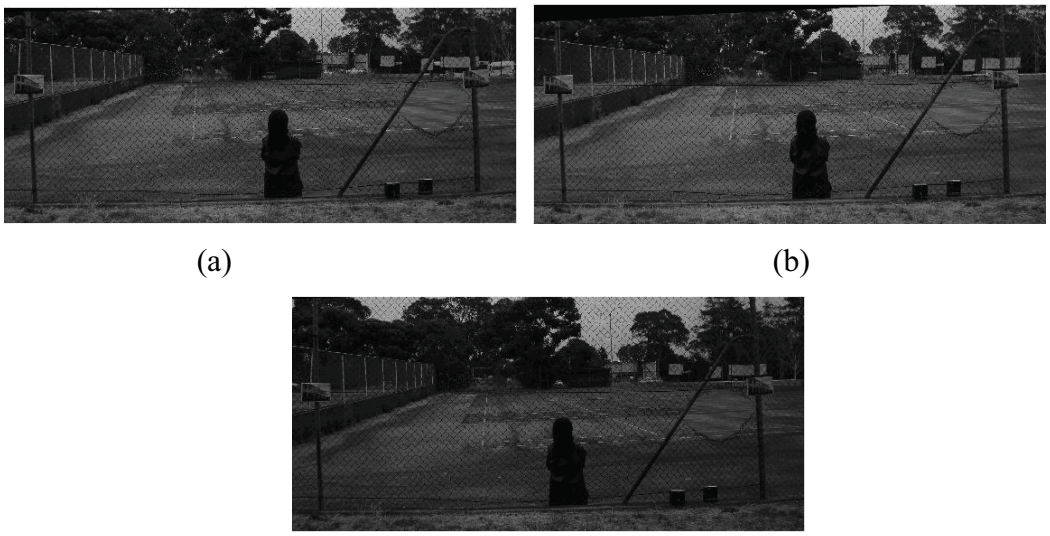

(a) (b)

(c)

Fig. 5.7 The ROI2_II-3 (a), ROI2_II-7 (b) and ROI2_II-11 (c) extracted from the RAOI1_II-3, RAOI1_II-7 and RAOI1_II-11 based on information of their own bounding box parameters

Figs. 5.8 (a), 5.8 (b) and 5.8 (c), below, depict results of image registration towards the AOI1_II-4, AOI1_II-8 and AOI1_II-12 by using CPs extracted from the images. Information regions are then split from black regions based on information of their bounding box parameters in order to produce the ROI2_II-4, ROI2_II-8 and ROI2_II-12 (see Figs. 5.9 (a), 5.9 (b) and 5.9 (c) below).

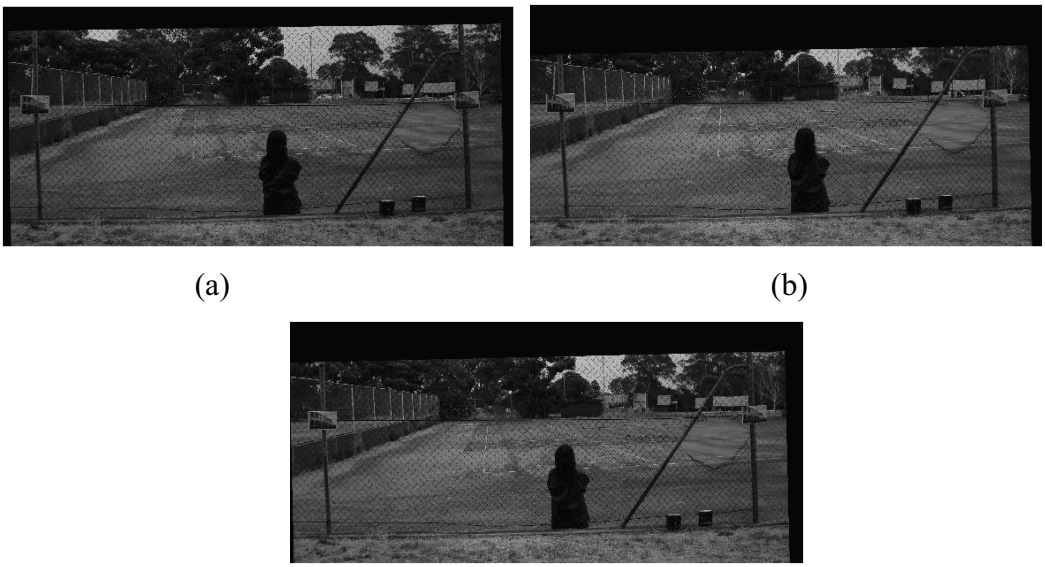

(a) (b)

(c)

Fig. 5.8 The RAOI1_II-4 (a), RaOI1_II-8 (b) and RAOI1_II-12 (c) produced after performing image registration

(a) (b)

(c)

Fig. 5.9 The ROI2_II-4 (a), ROI2_II-8 (b) and ROI2_II-12 (c) cropped from the RAOI1_II-4, RAOI1_II-8 and RAOI1_II-12 by using information of their bounding box parameters

Table 5.1 depicts translation, scaling and rotation values of each RAOI1_II. In term of translation, negative and positive values indicate movement in left and right directions for X axis, and down and up directions for Y axis. In term of scaling, negative and positive values changes in object's sizes whether to be smaller or bigger. In term of rotation, negative and positive values represent rotation in anticlockwise and clockwise.

Table 5.1 Summarization of translation, scaling and rotation values of each RAOI1_II

Position in Fig. 4.2	Registered Input Image	Translation (pixels)		Scaling (times)	Rotation (degree)
		X axis	Y axis		
1	RAOI1_II-1	- 6.0487	- 267.0800	1.0366	- 0.7888
5	RAOI1_II-5	39.9812	- 275.4772	1.0364	- 1.4329
9	RAOI1_II-9	62.7486	- 298.0080	1.0156	- 2.5098
2	RAOI1_II-2	70.0131	- 206.1381	0.9839	- 0.8755
6	RAOI1_II-6	51.8627	- 140.5212	1.0035	- 0.8730
10	RAOI1_II-10	87.3936	- 204.2860	0.9854	- 0.9386
3	RAOI1_II-3	79.2197	- 181.0356	0.9709	- 1.1984
7	RAOI1_II-7	119.1253	- 238.0314	0.9714	- 2.5900
11	RAOI1_II-11	90.5616	- 52.6736	0.9841	- 1.8475
4	RAOI1_II-4	- 29.0533	- 161.3944	1.0351	- 0.8491
8	RAOI1_II-8	32.0034	- 323.4566	1.0195	- 1.0954
12	RAOI1_II-12	10.3735	- 268.4688	1.0355	- 1.3310

As depicted in Table 5.1, object's sizes in all RAOI1_IIs haven't significantly changed since scaling values are around 1. Moreover, rotation in anticlockwise has slightly happened in all RAOI1_IIs. In contrast, translation in X and Y axes has considerably occurred in all RAOI1_IIs as a result of camera motion when capturing the multiple outdoor images. For instance, the RAOI1_II-1 has moved 6 and 267 pixels to the left and down directions, rotated 0.8 angles in anticlockwise and no changed in object's sizes in it. Little changes in scaling and rotation values show that CPs used to register RAOI1_IIs have a good accuracy. In other words, the template-

based matching approach applied in extracting CPs from these kinds of multiple outdoor images has a high success.

The aim of using image registration in this research is to reduce the influence of parallax in the reference image and input images. As a result of extracting only two CPs from left and right posts of the wire fence in the reference image and input images, left and right posts of the wire fence in the RAOI1_IIs are around in the same coordinate system with left and right posts of the wire fence in the reference image. Fig. 5.10, below, depicts a subtracted image between the ROI2_II-1 and the ROI2_RI-1 (see Figs. 5.2 (a) and 5.2 (b) above).

Fig. 5.10 The subtracted image between the ROI2_II-1 and the ROI2_RI-1

As can be observed in Fig. 5.10, left post of the wire fence is composed by two regions: black and white regions. The black region indicates that pixels of left post in both ROI2_II-1 and ROI2_RI-1 are in the same coordinate system. The white region represents pixels of left post in the ROI2_II-1 are around or close to pixels of left post in the ROI2_RI-1. In other words, the black region reveals a zero disparity region and the white region denotes a disparity region. Small disparities can also be observed in between fence wires. Moreover, the more objects are far from the wire fence, the larger disparities occur to the objects. This phenomenon can be used for further process in order to detect disappearing and/or appearing of objects behind the wire fence.

5.4 Concluding Remarks

CPs obtained from left and right posts of the wire fence in the reference image and input images are used as correspondence points in registering input images into the same coordinate system with the reference image. Each registered input image consists of black and information regions. To eliminate the black region from each registered input image, bounding box parameters of the information region are exploited by applying a global thresholding towards the registered input image.

The purpose of registering the reference image and input images is to decrease parallax. As a result, pixels at and/or around CPs often have zero and/or small disparities, vice versa, in a subtracted image of the reference image and the registered input image. These observable facts are investigated further in this research in detecting presence and/or absence of objects behind the wire fence.

CHAPTER 6

CONFIDENCE MAP AND OCCLUSION MAP IMAGES GENERATION

Chapter 6 explains a process of generating confidence map and occlusion map images from the ROI2_RIs and ROI2_IIs. The explanation begins with reasons of using confidence map and occlusion map images in the field of change detection research. Algorithms of making confidence map and occlusion map images are described in the next two sections. Experimental results and discussion are then presented in the further section. Concluding remarks are drawn in the final section of this chapter 6.

6.1 Background

In the case of registering two or more depth plane images, gaps, known also as disparities, apparently appear in pixels of same objects in both the reference and registered input images (Russ, 2002). Disparities of pixels at and/or close to CPs are zero and/or small, vice versa, pixels that are far away from CPs have larger disparities. These situations can be observed in the subtracted image between the ROI2_RI and ROI2_II-1 as shown in Fig. 5.10 (see Chapter 5). These disparities are then investigated further in this research.

Stereo correspondence algorithms can be utilized in producing disparity and/or confidence maps (Scharstein and Szeliski, 2002). A disparity map represents disparity estimates of pixels and a confidence map represents confidences of matched pixels. In making disparity and/or confidence maps, most stereo correspondence algorithms do not take into account occlusion openly (Zitnick and Kanade, 2000). There are several methods that have attempted to explicitly detect occlusions, including methods using intensity edges (Intille and Bobick, 1994), multiple cameras with camera masking (Nakamura, *et al.*, 1996),

bi-directional matching (Fua, 1993) and the magnitude of the converged match values examination in conjunction with the uniqueness constraint (Zitnick and Kanade, 2000).

In change detection, appearing and disappearing of objects in multiple images of the same scene captured by a mobile camera could be represented as occlusion regions in a disparity or confidence map. Finding occlusion regions in a disparity or confidence map is emphasized in this research, especially occlusion regions around the wire fence. As expected, disparities around the wire fence will be zero or small as CPs are extracted from left and right posts of the wire fence and disparities on background of the scene will be large. As a focus of this research is to detect presence and/or absence of objects behind the wire fence, this study is only focus on how to extract occlusion regions around the wire fence.

6.2 Confidence Map Image Making

In this study, a cooperative algorithm (Zitnick and Kanade, 2000), referred to as the Zitnick and Kanade algorithm (ZKA), was used to produce a confidence map image (i.e., an image that displays the confidence that match values are correct). The ROI2_RI and ROI2_II as explained in Chapter 5 were used as inputs. Parameters used by the ZKA during the experiment are summarized in Table 6.1 below.

Table 6.1 Summarization of the ZKA parameters used in this study

No.	Parameters	Values
1	Minimum Disparity	0
2	Maximum Disparity	8
3	WinRadL0	1
4	WinRadRC	2
5	WinRadD	1
6	NumIterations	5
7	MaxScaler	0.96
8	Matching Operator	Sums of Absolute Differences (SAD)

where WinRadL0 is window radius used for computing the initial match values (L_0). WinRadRC and WinRadD are local support radiuses (row-column

dimensions) and (disparity dimension) used for averaging match values during each iteration. NumIterations is number of iterations used to refine the disparity map. MaxScaler is used for linearly scaling the L_0 values when SAD is used. SAD is used to compute the L_0 values.

The ZKA is an iterative algorithm that can be used for obtaining disparity maps with occlusion explicitly detected. In other words, the ZKA also produces confidence maps that depict the confidences of match values, which are correct. The confidence is determined by how good a score of a point is received when its window is matched to another image.

When some objects in the first image are occluded in the second image, or vice versa, pixels that do not have matched pixels will get minimum match values. If the minimum match values are lower than or equal to a threshold, the pixels will be classified as occluded. In confidence maps, pixels categorized as occluded will be set up into black colour regions. The ZKA is summarized as follows (Zitnick and Kanade, 2000):

1. Prepare a 3D array, (*r, c, d*): *(r, c)* corresponds to each pixel in the ROI2_RI and *d* for the range of disparity.
2. Set initial match values L_0 using a function of image intensities, such as squared differences or normalized correlation.
3. Iteratively update match values L_n using equation (6.5) after combining equations (6.1), (6.2), (6.3) and (6.4) in their respective order, until the match values converge (Zitnick and Kanade, 2000).

$$L_0(r,c,d)=\delta(I_{ROI2\_RI},I_{ROI2\_II},r,c,d) \tag{6.1}$$

$$S_n(r,c,d)=\sum_{(r',c',d')\in\Phi} L_n(r+r',c+c',d+d') \tag{6.2}$$

$$R_n(r,c,d)=\left(\frac{S_n(r,c,d)}{\sum_{(r'',c'',d'')\in\Psi(r,c,d)} S_n(r'',c'',d'')}\right)^{\alpha} \tag{6.3}$$

$$T_n(r,c,d)=L_0(r,c,d)*R_n(r,c,d) \tag{6.4}$$

$$L_{n+1}(r,c,d) = L_0(r,c,d) * \left(\frac{S_n(r,c,d)}{\sum_{(r'',c'',d'') \in \Psi(r,c,d)} S_n(r'',c'',d'')} \right)^{\alpha} \tag{6.5}$$

where $L_n(r,c,d)$ is the match value assigned to element (r,c,d) at iteration *n*, $L_0(r,c,d)$ is the initial values, δ is an image similarity function such as squared differences or normalized correlation at windows centered on (r,c) and $(r,c+d)$, $S_n(r,c,d)$ is the amount of local support for (r,c,d) (i.e., the sum of all match values within a 3D local support area, Φ), $R_n(r,c,d)$ is the amount of inhibition $S_n(r,c,d)$ received from the elements in $\Psi(r,c,d)$, α is used to control the amount of inhibition per iteration, $T_n(r,c,d)$ is the value $R_n(r,c,d)$ restricted by $L_0(r,c,d)$ and * is a multiplying process.

4. For each pixel (*r, c*), find the element (*r, c, d*) with the maximum match value.
5. If the maximum match value is higher than a threshold (i.e., the threshold for detecting occlusions was set constant for all image pairs at 0.005), output the disparity *d*, otherwise classify it as occluded.

Each match value, whether or not it categorizes as disparity or occluded, is normalized into an intensity value in the confidence map image. Match values classified as disparities are normalized into lighter areas (higher intensity values), vice versa. As a result, there are two distinctive areas in the confidence map image: lighter and darker areas. Lighter areas represent high confidence values as disparity and darker areas symbolize occlusion regions. This study is only emphasized in extracting darker areas in the confidence map image since these darker areas contain potential significant changes (disappearing and/or appearing of objects behind the wire fence in the scene).

6.3 Occlusion Map Image Making

Stereo correspondence algorithms often produce two maps: disparity and confidence. In this study, a new map is introduced and referred to as an occlusion

map image (OMI). The OMI is a binary image and it only contains occluded regions extracted from the confidence map image. The OMI algorithm is outlined below:

1. Perform brightness thresholding to a confidence map image. Let us define $C(x, y)$ to be the confidence map image, a binary image, $B(x, y)$, was produced by equation (6.6).

$$B(x,y)=\begin{cases}1 if\ C(x,y)=\tau \\ 0 if\ C(x,y)\neq\tau\end{cases} \tag{6.6}$$

   where τ is the threshold values established constantly at 39 and 40 for any confidence map image. The τ values were experimentally decided based on information of the image histogram of the confidence map image. Occluded regions were represented at darker areas in the confidence map image, hence, searching of τ values was limited in darker parts (0 – 50 intensity values). The first and second highest peaks in the image histogram were chosen as τ values.
2. Remove objects whose areas are less than ρ pixels. A binary image, $B_2(x, y)$, was generated by using equation (6.7), below.

$$B_2(x,y)=\begin{cases}B(x,y) if\ B(x,y)>\rho \\ 0 \qquad otherwise\end{cases} \tag{6.7}$$

   where ρ is the area of an object (i.e., the number of pixels in the region) in $B(x, y)$ whose value was limited to between 700 to 16000 pixels. These values were set constant for any confidence map image. The ρ values correspond to the actual areas of objects depending on the distance between the objects and the camera and it was experimentally determined based on information summarized in Table 6.2, below. In the Table 6.2, F_s is the file size of an original input image in megabyte (MB) and C_d is the distance of a mobile-camera to an outdoor wire fence.

Table 6.2 Summarization of ρ values

ρ (pixels)	F_s **(MB)**	C_d **(m)**
[700, 16000]	8	6
[260, 870]	4	6
[503, 1113]	4	5
[746, 1356]	4	4
[1000, 1600]	4	3

3. Remove objects whose eccentricity (i.e., the ratio of the distance between the foci of the ellipse and its major axis length) are greater than ε. A binary image, $B_3(x, y)$, was generated by using equation (6.8), below.

$$B_3(x,y)=\begin{cases} B_2(x,y) \; if \; B_2(x,y)<\varepsilon \\ 0 \qquad otherwise \end{cases} \tag{6.8}$$

where ε is the eccentricity value set constant for any at $B_2(x, y)$ 0.98 in this study. This value indicated that the form of an object was a line shape. This step removed objects generated by straight line wires of the fence.

4. Perform a dilation technique (Gonzalez and Woods, 2008) to $B_3(x, y)$ in generating an OMI, $B_4(x, y)$.

6.4 Experimental Results and Discussion

As mentioned in Section 6.2, above, the ROI2_RIs and ROI2_IIs are used as inputs by the ZKA in producing confidence map images. Figs. 6.1 (a), 6.1 (b) and 6.1 (c), below, depict confidence map images (CMIs) produced by the ZKA. The ROI2_RI-1 (i.e., a region of interest extracted from the reference image based on information of bounding box parameters of the RAOI1_II-1) and ROI2_II-1 were used as inputs by the ZKA to generate a CMI referred to as CMI_II-1 (see Fig. 6.1 (a), below). The ROI2_RI-5 and ROI2_II-5 were used by the ZKA as inputs in making a CMI_II-5 in Fig. 6.1 (b), below. To generate a CMI_II-9, the ZKA used the ROI2_RI-9 and ROI2_II-9 as inputs (see Fig. 6.1 (c), below).

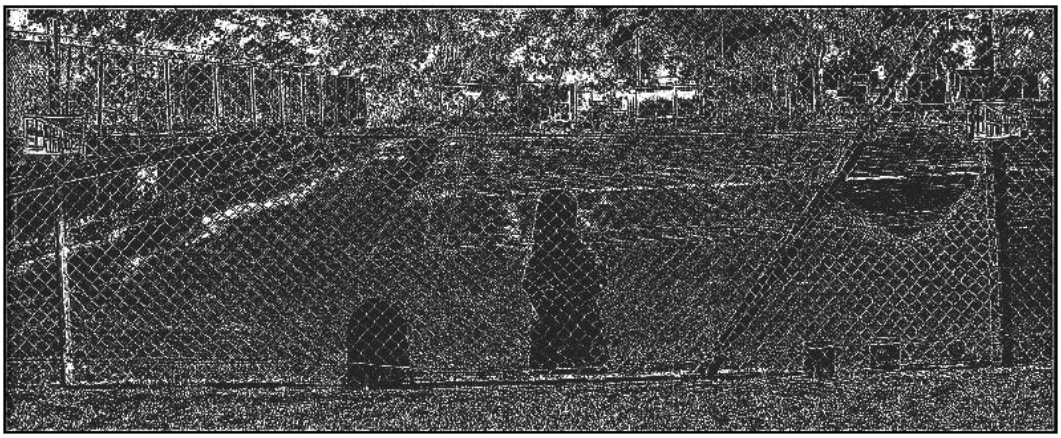

(a)

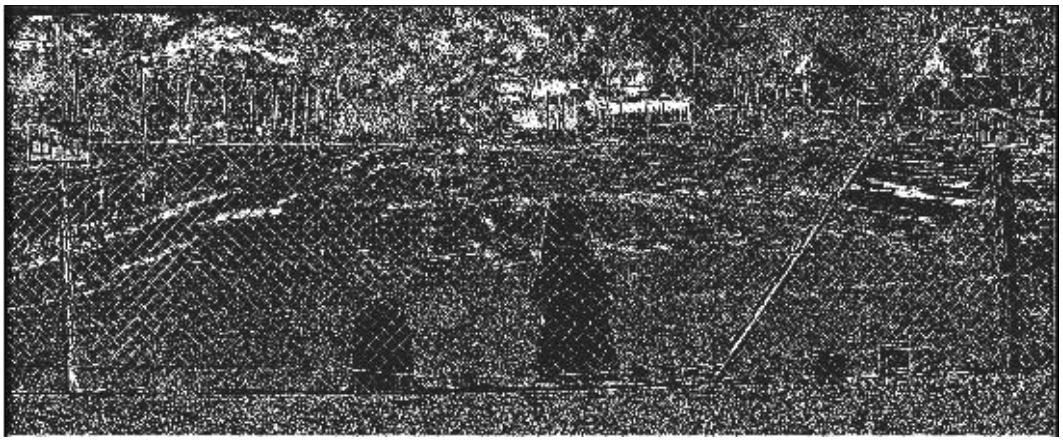

(b)

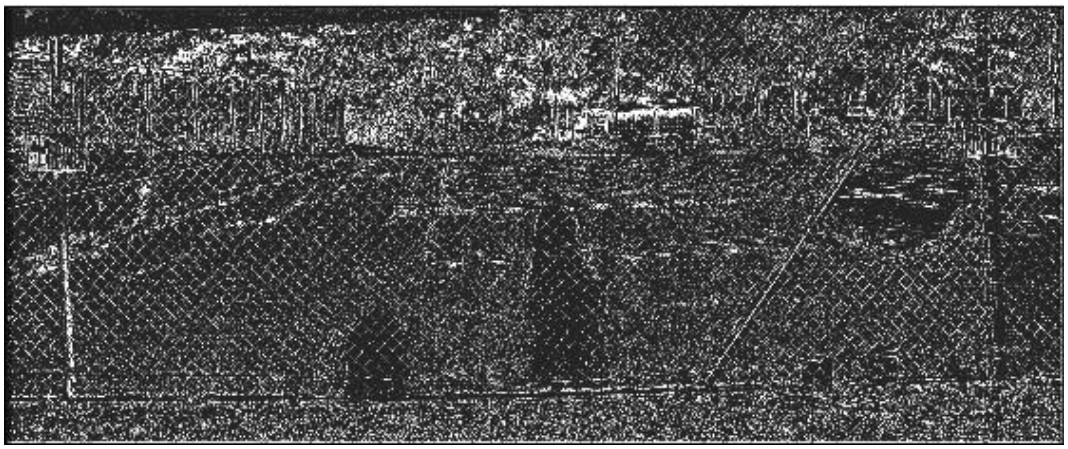

(c)

Fig. 6.1 The CMI_II-1 (a), CMI_II-5 (b) and CMI_II-9 (c) produced by the ZKA

As seen in Figs. 6.1 (a), 6.1 (b) and 6.1 (c), above, there are two distinctive areas in each CMI: lighter and darker areas. Lighter areas vary in the CMIs because of illumination variations that occur on the CMIs. Although the ROI2_II-1, ROI2_II-

5 and ROI2_II-9 were captured by a mobile camera from slightly different positions, angles and at slightly different times, intensity values of the images will vary as a result of camera movement and varying illumination. Right posts of the wire fence in the CMIs are dark areas. It depicts that right posts of the wire fence in the ROI2_II-1, ROI2_II-5 and ROI2_II-9 are in the same coordinate system with right posts of the wire fence in the ROI2_RI-1, ROI2_RI-5 and ROI2_RI-9. On the other hand, these situations do not occur with left posts of the wire fence since left posts of the wire fence are in lighter areas in the CMIs. It observably appears from the CMIs that presence and absence of objects, especially an intruder and a school back, are presented in darker areas as these darker areas are focus in the further process.

Figs. 6.2 (a), 6.2 (b) and 6.2 (c), below, depict a CMI_II-2, CMI_II-6 and CMI_II-10 generated by the ZKA.

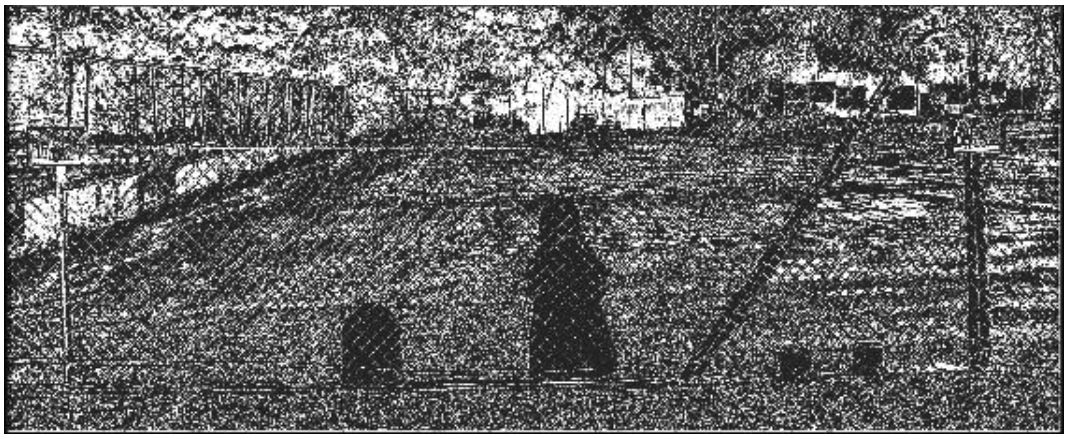

(a)

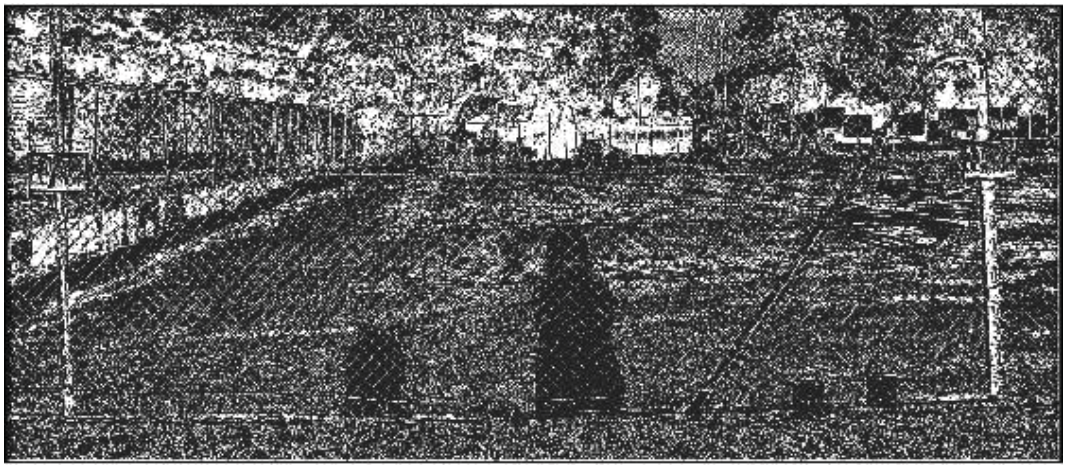

(b)

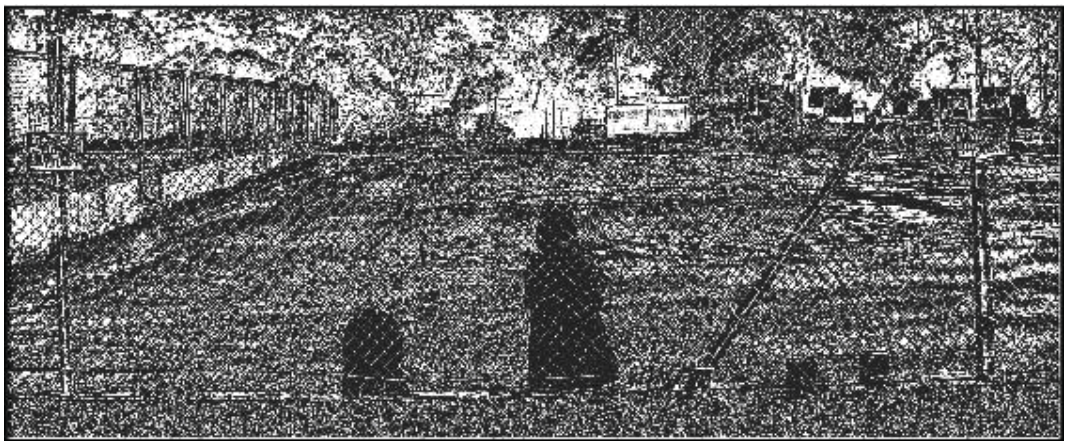

(c)

Fig. 6.2 The CMI_II-2 (a), CMI_II-6 (b) and CMI_II-10 (c) produced by the ZKA

The ROI2_RI-2 and ROI2_II-2 (i.e., regions of interest cropped automatically from the AOI1_RI and RAOI1_II-2 based on information of the RAOI1_II-2's bounding box parameters) were used by the ZKA in producing the CMI_II-2 (see Fig. 6.2 (a)), etc. More lighter areas observably appear in the CMI_II-2, CMI_II-6 and CMI_II-10 rather than in the CMI_II-1, CMI_II-5 and CMI_II-9. It occurs as the AOI1_II-2, AOI1_II-6 and AOI1_II-10 were captured by a mobile camera from slightly different positions, angles and at different times (around two hours after capturing the AOI1_II-1, AOI1_II-5 and AOI1_II-9).

Figs. 6.3 (a), 6.3 (b) and 6.3 (c), below, depict a CMI_II-3, CMI_II-7 and CMI_II-11 produced by the ZKA by using the ROI2_RI-3 and ROI2_II-3, the ROI2_RI-7 and ROI2_II-7, and the ROI2_RI-11 and ROI2_II-11 as inputs.

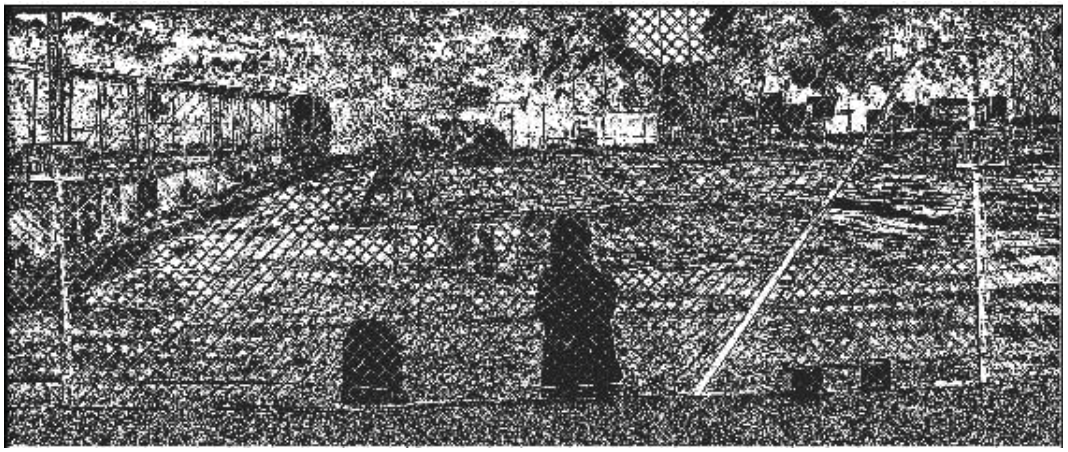

(a)

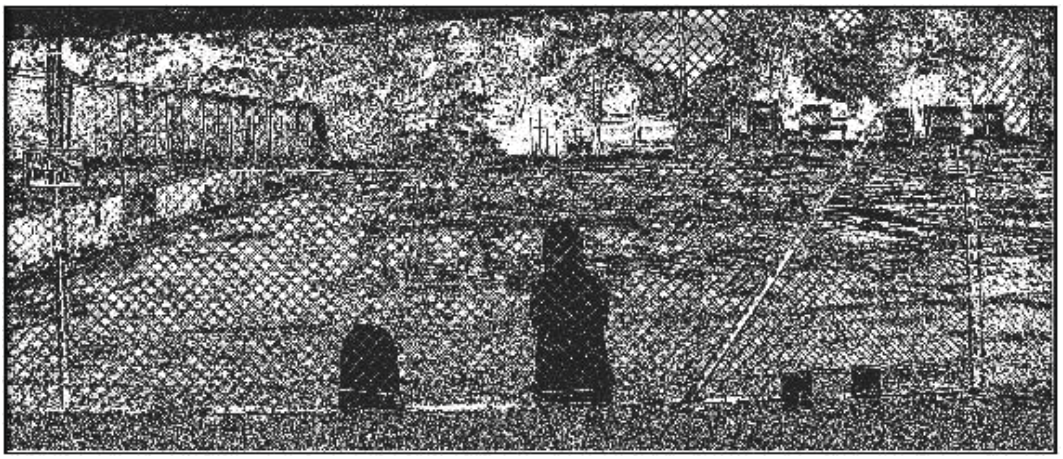

(b)

(c)

Fig. 6.3 The CMI_II-3 (a), CMI_II-7 (b) and CMI_II-11 (c) generated by the ZKA

As seen in Figs. 6.3 (a), 6.3 (b) and 6.3 (c), lighter areas vary in each CMI. Extra lighter areas apparently appear in the CMI_II-3 and CMI_II-7 rather than in the CMI_II-11.

Figs. 6.4 (a), 6.4 (b) and 6.4 (c), below, depict a CMI_II-4, CMI_II-8 and CMI_II-12 produced by the ZKA. More lighter areas observably appear in the CMI_II-4 instead of in the CMI_II-8 and CMI_II-12. Contours of the school bag and the intruder apparently appear in each CMI. In further process, darker areas are extracted from all CMIs since darker areas could contain potential significant changes (i.e., appearing and/or disappearing of objects behind the wire fence).

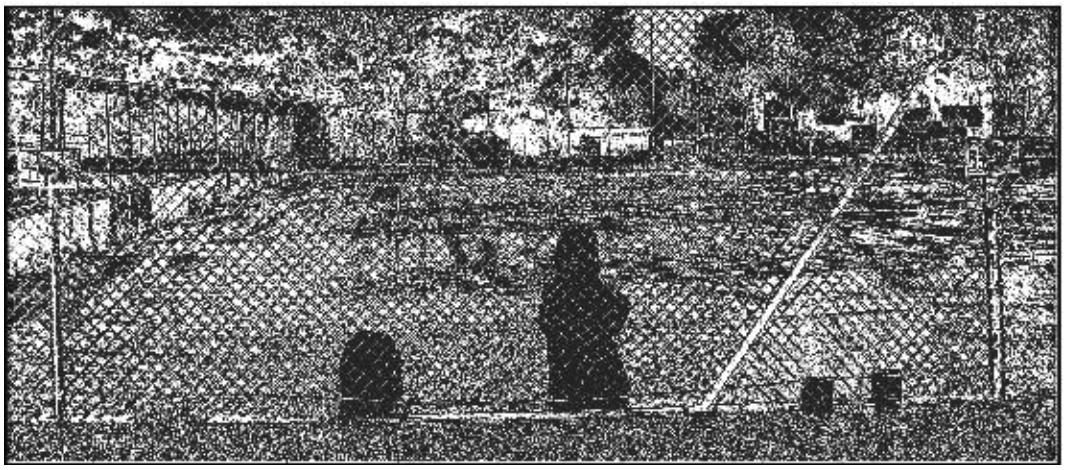

(a)

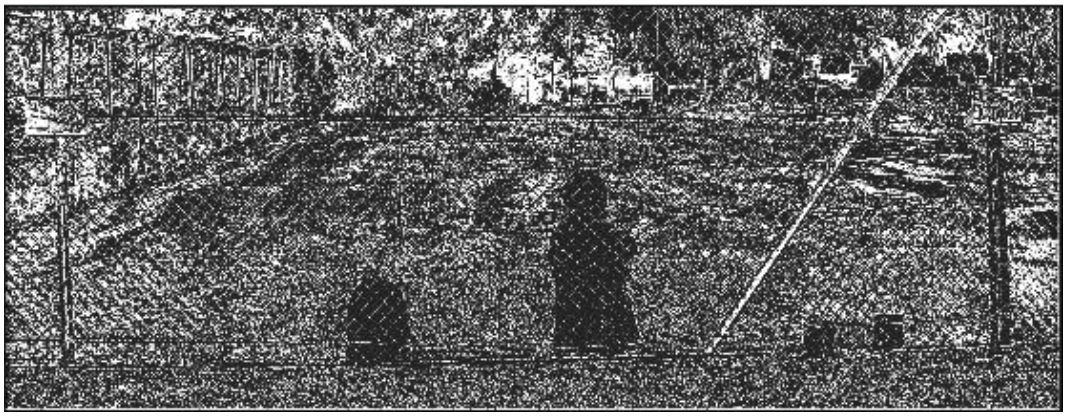

(b)

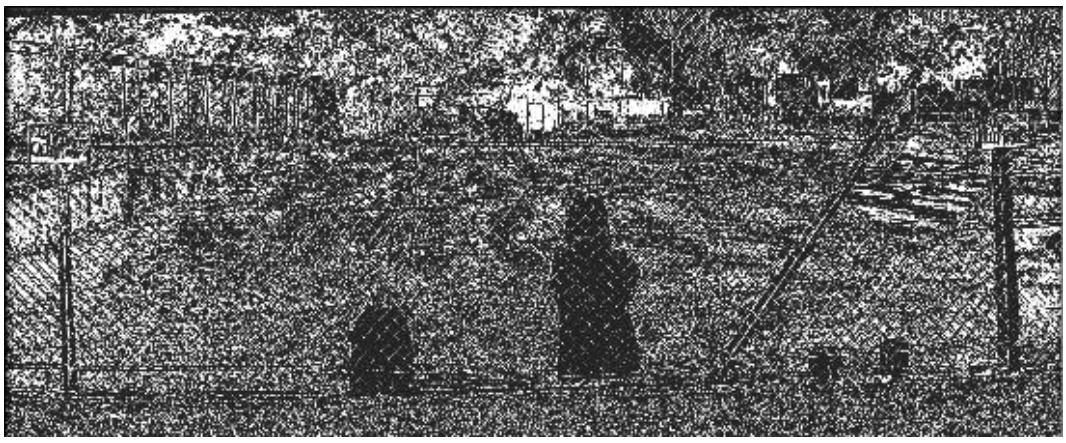

(c)

Fig. 6.4 The CMI_II-4 (a), CMI_II-8 (b) and CMI_II-12 (c) produced by the ZKA in which the ROI2_RI-4 and ROI2_II-4, the ROI2_RI-8 and ROI2_II-8, and the ROI2_RI-12 and ROI2_II-12 were used as inputs

The next process is to extract occluded regions (darker areas) from CMIs, above, in order to generate OMIs. Steps in Section 6.3, above, were applied into

CMIs. The following is a completed explanation of how to produce the OMI_II-1 from the CMI_II-1. First of all, brightness thresholding was performed into the CMI_II-1 in which threshold values were 39 and 40. Fig. 6.5, below, depicts the result of brightness thresholding towards the CMI_II-1.

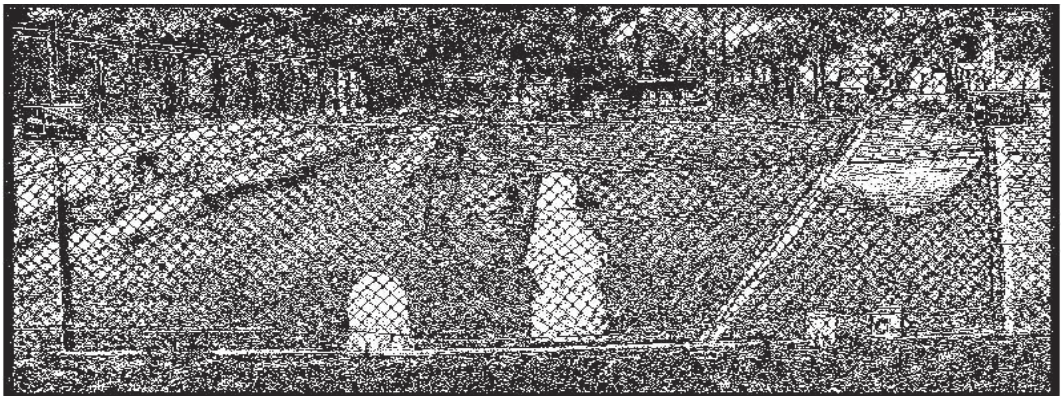

Fig. 6.5 A binary image of the CMI_II-1 after performing brightness thresholding

As seen in Fig. 6.5, darker areas are converted to white pixels. Big objects such as the school bag and intruder are separated into many small regions by edges of fence wires. Horizontal and vertical-shaped objects (horizontal and vertical posts of the wire fence) observably appear as well.

Secondly, small and big objects were separated from the binary image based on information of theirs sizes in pixels. The sizes in pixels used in this study are the range of 700 – 16,000 pixels. Objects that have sizes bigger and smaller than the range were removed from the binary image, vice versa. Fig. 6.6, below, depicts the result of separating objects based on their areas in pixels.

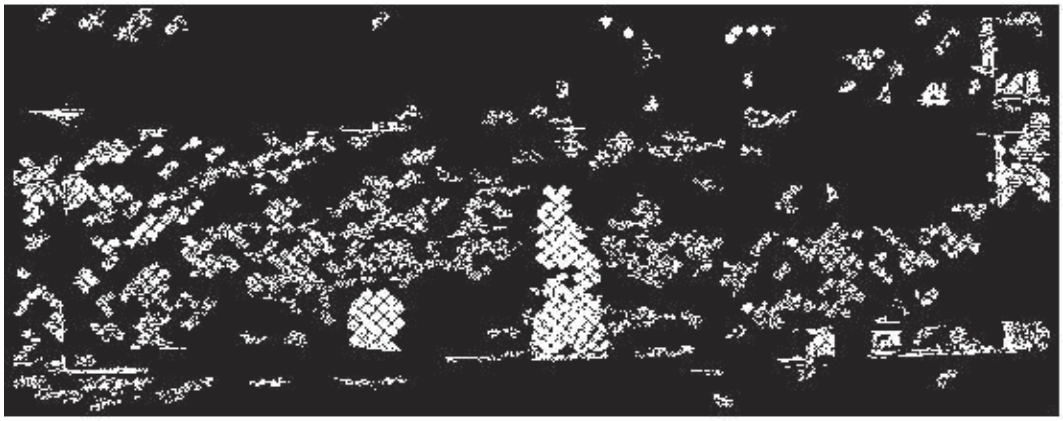

Fig. 6.6 Objects whose sizes in the range of 700 – 16,000 pixels

Thirdly, line-shaped objects were eliminated from the image in Fig. 6.6, above, based on information of their eccentricity values. Objects that have eccentricity values equal or greater than 0.98 were removed. Fig. 6.7, below, depicts the result of removing objects based on their eccentricity values.

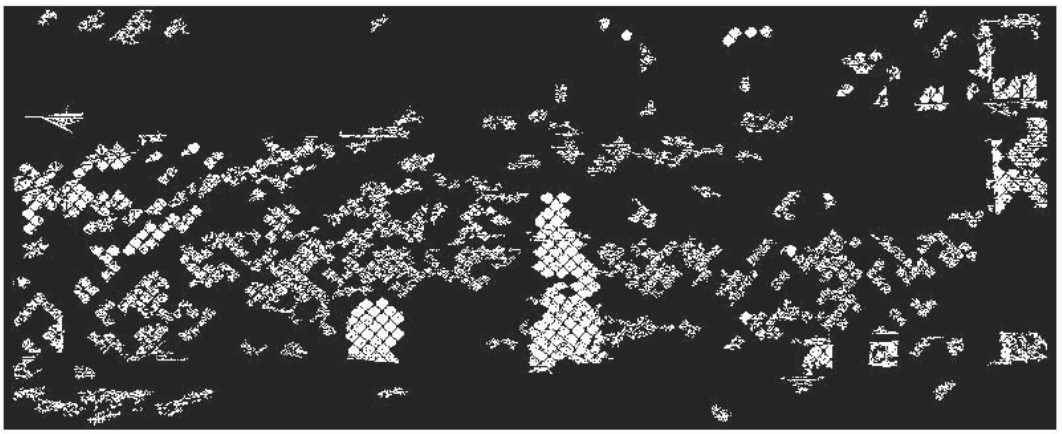

Fig. 6.7 Objects whose eccentricity values lower than 0.98

Finally, a dilation process was performed on the image in Fig. 6.7 in order to unite separated small objects into big objects. Fig. 6.8, below, depicts the final image as a result of the dilation process. This final image is referred to as an OMI_II-1.

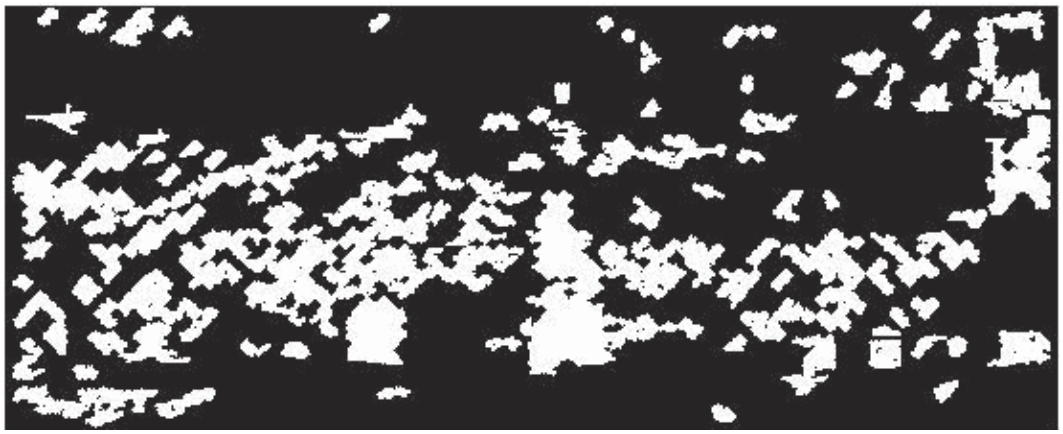

Fig. 6.8 The OMI_II-1 produced from the CMI_II-1

The same steps were then applied to other CMI_IIs in generating other OMIs. The following Figs. depict other OMI_IIs.

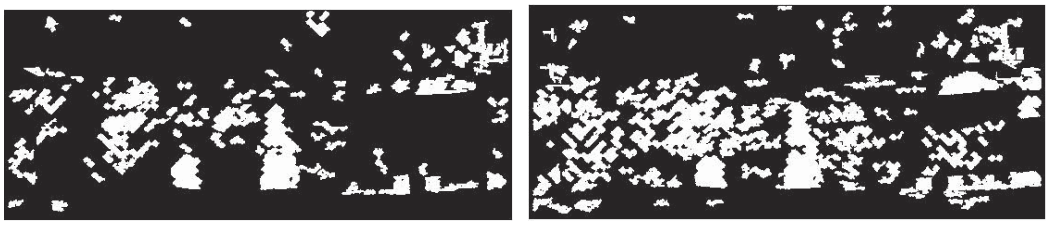

(a) (b)

Fig. 6.9 The OMI_II-5 (a) and OMI_II-9 (b)

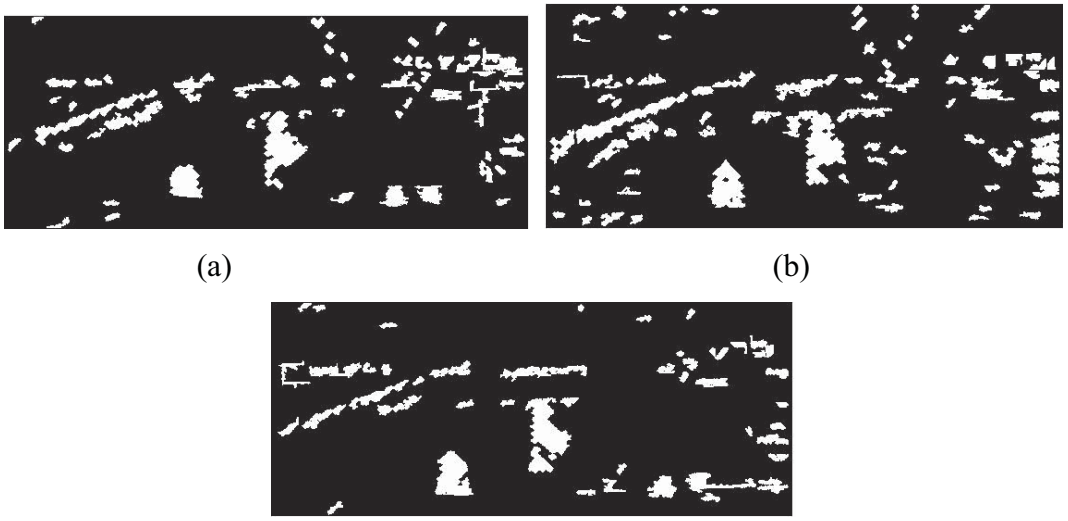

(a) (b)

(c)

Fig. 6.10 The OMI_II-2 (a), OMI_II-6 (b) and OMI_II-10 (c)

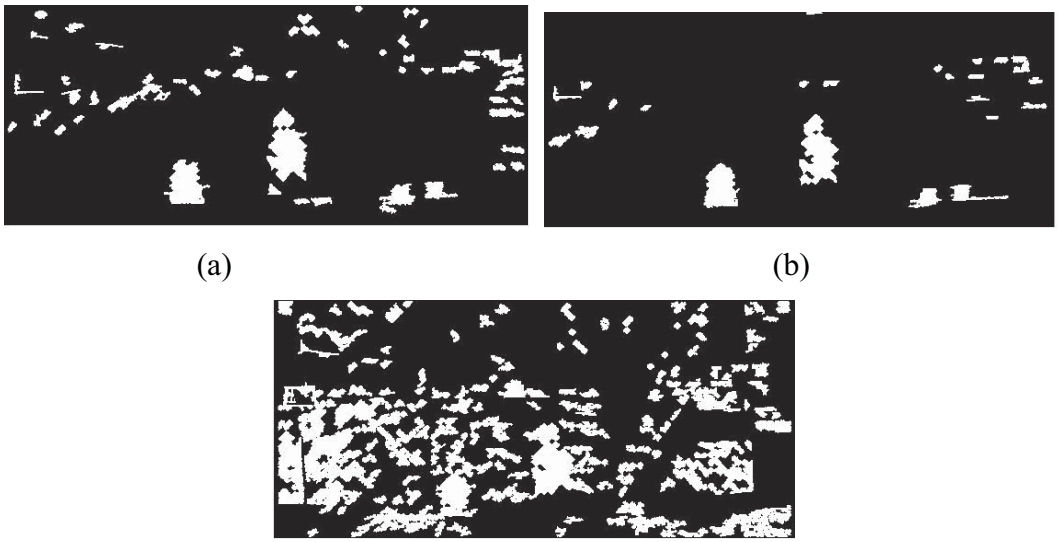

(a) (b)

(c)

Fig. 6.11 The OMI_II-3 (a), OMI_II-7 (b) and OMI_II-11 (c)

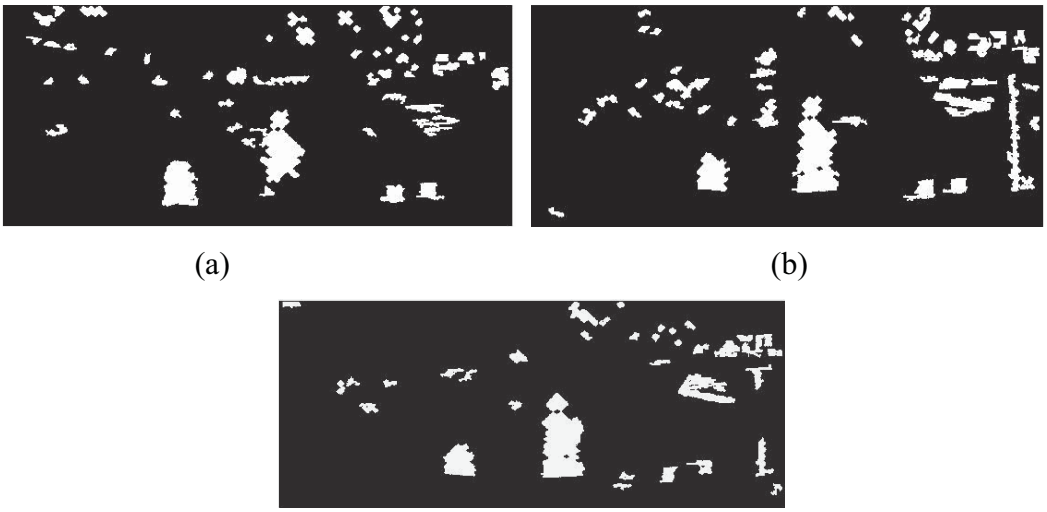

(a) (b)

(c)

Fig. 6.12 The OMI_II-4 (a), OMI_II-8 (b) and OMI_II-12 (c)

As seen in OMI_IIs, above, white pixels represent objects that could be either unimportant or significant changes. Unimportant and significant changes (i.e., a school bag and an intruder) have distinctive contours and sizes in pixels. Some OMIs (e.g., OMI_II-1, OMI_II-5, OMI_II-9 and OMI_II-11 (see Fig. 6.8, Figs. 6.9 (a), 6.9 (b) and Fig. 6.11 (c)) have complex occluded regions.

Based on information of object properties - width, height, eccentricity and area - in each OMI_II, these objects can be separated into unimportant or significant changes. An intelligent decision-making system is developed in further process in deciding which objects in each OMI_II belong to unimportant or significant changes.

6.5 Concluding Remarks

Disparities that occur in the ROI2_RIs and ROI2_IIs are investigated further in this chapter. A stereo correspondence algorithm known as the Zitnick and Kanade algorithm (ZKA) is utilized in this research in order to produce CMIs. In each CMI, matched values are represented in lighter pixels and occluded regions are depicted in darker pixels. Darker pixels are investigated further in the next process since they could contain potential significant changes (absence and/or presence of objects in the scene).

Occluded regions are then extracted from each CMI by performing the occlusion map image generating algorithm. Objects in each OMI_II have specific properties such as width, height, eccentricity and area. Based on these object properties, objects in each OMI_II can be classified into unimportant or significant changes. In order to classify objects in each OMI_II that belong to unimportant or significant changes, a first hyrid decision-making system is developed in this research and will be discussed in the next chapter.